

Computation of Cavitating Flow through Marine Propulsors

Jules W. Lindau, William L. Moody, Michael P. Kinzel, James J. Dreyer,
Robert F. Kunz, Eric G. Paterson

The Pennsylvania State University, Applied Research Laboratory, State College, PA, 16804

ABSTRACT

Computed single phase and cavitating flow fields are presented for two open propellers and a ducted waterjet. Modeling is performed using a Reynolds-Averaged Navier-Stokes solver with homogenous-multiphase modeling and turbulent simulation capabilities. The open propeller computations include both steady, uniform inflow computations as well as unsteady, distorted inflow, conditions. The ducted waterjet computations assume steady, periodic flow conditions with body forces to represent the effect of the downstream stator row. Computed performance parameters and cavity shapes are compared with experimental observations.

KEYWORDS

CFD, RANS, Cavitation, Multiphase Flow.

1 INTRODUCTION

Marine propulsor flow fields are inherently unsteady and three-dimensional. Propulsor performance, like nearly all turbomachinery, is influenced by flows that are rotational, viscous, and turbulent. Open propellers, for surface ships, typically operate in a nonuniform wake-dominated flowfield. Ducted propulsors, such as water jets, are influenced by numerous interacting shear flows. Water jet flows, due to hub, shroud, tip gap, and stator regions, tend to be more strongly influenced by shear flows and interacting vortical structures than open propellers. For all propulsors, cavitation, due to local pressure depressions is a persistent condition of interest. Typically, cavitation is a limiting condition on propulsor performance. This may be due to an absolute level of loading that may not be exceeded, resulting in a limit on thrust, i.e. thrust breakdown.

A three-dimensional, multiphase Reynolds-Averaged, Navier-Stokes (RANS) computational tool is applied to propeller flow computations, both steady and unsteady. Previously, Kunz et al. (2000) and Lindau et al. (2005) have presented steady and unsteady cavitating flow results using the locally homogeneous RANS approach. The results of Lindau et al. (2005) represented the flow of an unducted marine propeller over a wide range of advance ratios from fully wetted operating conditions through cavitation driven thrust breakdown. The large scale of such cavities implies tractability by a

homogeneous approach. Nonetheless, they are generally unsteady, and contain regions of separated flow. In flows modeled here, interface curvatures are small, and pressure and velocity are approximately continuous across the interface. Thus, it is presumed that nonequilibrium interface dynamics are of negligible magnitude, and the effect of surface tension is not incorporated. For cavitation inception, where physics of tiny bubbles and nucleation is critical, this methodology would not be appropriate. For cloud cavitation, or cases where cavitation is sufficient to effect hydrodynamic performance, however, this homogeneous, single-fluid, multiphase approach is reasonable.

2 FORMULATION AND SOLUTION METHOD

To solve the locally homogeneous, multiphase flow, conservation equations, a structured, finite-volume formulation with formal third order spatial and second order temporal accuracy was employed. For much of the presented results, overset grids were also employed. Overset modeling was enabled using SUGGAR and DiRTlib (Noack 2005(1,2)). The differential form of the computational model in Cartesian tensor notation is given in Eqn. 1. The corresponding conservative variables, primitive variables, flux vectors, and source terms are also defined in Eqn. 1. The term $\Gamma^p \partial Q / \partial \tau$ is a result of the dual-time preconditioning approach (Venkateswaran et al. 2002). Steady cases were modeled in the rotating reference frame and include assumed periodicity about a single rotor blade. The noninertial, rotating frame term is indicated in the source vector of Eqn. 1. Unsteady cases were modeled in the inertial reference frame with grid velocities applied in the finite volume formulation.

To numerically capture very low Mach number, i.e. incompressible, flows, the inherent decoupling of the physical momentum and continuity equations may be resolved by various strategies (Venkateswaran and Merkle 1999). Here, a preconditioner is applied to yield a well conditioned inviscid eigensystem. The preconditioning matrix Γ^p appearing in Eqn. 1 was derived in Venkateswaran et al. (2002). The modified inviscid eigensystem then, ideally, dominates convergence of the pseudo-time marching system. Using the dual time approach, time accurate solutions are

obtained by marching in pseudo-time over each physical time step and driving the time accurate residual, the discrete form of the physical equations, to a small value. The coupled equations presented in Eqn. 1 are termed isothermal. The isothermal form admits compressibility of the liquid and gas species, but only as each species density may be a function of one independent variable, the local pressure. Thus each phase or species is assumed to have a constant sound speed. However, the mixture sound speed (and density) is strongly dependent on the local volume fraction composition. A fully compressible extension, one admitting dependence of properties on temperature, of the present formulation has been similarly derived (Lindau 2001) and is useful in consideration of extremely high speed flows and other thermal effects. Solutions presented here either assume either infinitesimal (10^{-15}) or very small (but physically correct) free stream Mach numbers. For steady computations at the low physical free stream Mach number conditions considered, the effect of compressibility is expected to be insignificant. However, it is expected that, even for very small free stream speeds, unsteady cavitating computations may be affected by compressibility (Venkateswaran et al. 2002).

$$\begin{aligned} \frac{\partial Q_c}{\partial t} + \Gamma^p \frac{\partial Q}{\partial \tau} + F_{j,j} - F_{j,j}^v &= H \\ Q &= \begin{bmatrix} p \\ u_j \\ \alpha_v \end{bmatrix} \quad Q_c = \begin{bmatrix} \rho \\ \rho u_j \\ \tilde{\rho}_v \alpha_v \end{bmatrix} \\ F_j &= \begin{bmatrix} \rho u_j \\ \rho u_i u_j + p \delta_{ij} \\ \tilde{\rho}_v \alpha_v u_j \end{bmatrix} \quad F_j^v = \begin{bmatrix} 0 \\ t_{ij} \\ 0 \end{bmatrix} \\ H &= \begin{bmatrix} 0 \\ -\rho [\varepsilon_{ijk} \omega_j \varepsilon_{klm} \omega_l x_m - 2\varepsilon_{ijk} \omega_j x_k] \\ -(\dot{m}^+ + \dot{m}^-) \end{bmatrix} \end{aligned} \quad (1)$$

It is convenient in the formulation used here to present continuity in the form of a mixture mass conservation law. This is apparent in Eqn. 1. Note that for all results presented here, only two phases are considered, a liquid and a vapor. Therefore, the subscript l is used to refer to liquid and v refers to vapor. When other gases or liquids are modeled as part of the local mixture, their inclusion, in the form of Eqn. 1, is a straightforward extension. The mixture density is defined based on the local volume average density.

$$\rho = \alpha_v \tilde{\rho}_v + \alpha_l \tilde{\rho}_l \quad (2)$$

The viscous stress tensor takes on the usual form for the mixture.

$$t_{ij} = \mu_{m,t} \left(u_{i,j} + u_{j,i} - \delta_{ij} \frac{2}{3} u_{k,k} \right) \quad (3)$$

In Eqn. 4, necessary mixture turbulent and molecular viscosities are defined. Where applied, the subscript m indicates a liquid-gas mixture quantity. As is sensible, the mixture molecular viscosity is based on a local volume average. The eddy viscosity is defined to be consistent with the locally homogeneous mixture assumption.

$$\begin{aligned} \mu_t &= \frac{\rho C_\mu k^2}{\varepsilon} \\ \mu_m &= \alpha_l \mu_l + \alpha_v \mu_v \\ \mu_{m,t} &= \mu_m + \mu_t \end{aligned} \quad (4)$$

A two-equation turbulence closure model is employed. At each pseudo-time step, these are solved in a segregated manner, from the flow equations, and are presented in Eqn. 5. The production term, P , is the product of the product of the velocity derivative and stress tensors. Also, for solutions containing near-wall grid resolutions, a damping parameter controls the modeled production and eddy viscosity in near-wall regions of the flow. Otherwise it approaches unity. (Abdol-Hamid et al. 1995). Standard values for other constants, C_1 and C_2 , are applied (Wilcox 1998). For unsteady computations, a DES variant is employed (Kinzel 2007).

$$\begin{aligned} \frac{\partial Q_T}{\partial t} + \frac{\partial F_j^T}{\partial x_j} &= PROD - DEST \\ Q_T &= \begin{bmatrix} \rho k \\ \rho \varepsilon \end{bmatrix} \\ F_j^T &= \begin{bmatrix} \rho k u_j - \left(\mu_m + \frac{\mu_t}{\sigma_k} \right) \frac{\partial k}{\partial x_j} \\ \rho \varepsilon u_j - \left(\mu_m + \frac{\mu_t}{\sigma_\varepsilon} \right) \frac{\partial \varepsilon}{\partial x_j} \end{bmatrix} \\ PROD &= \begin{bmatrix} 1 \\ C_1 \frac{\varepsilon}{k} \end{bmatrix} \rho P \\ DEST &= \begin{bmatrix} \rho \varepsilon \\ C_2 \rho \frac{\varepsilon^2}{k} \end{bmatrix} \end{aligned} \quad (5)$$

The transfer of mass between liquid and vapor states is handled with simple finite-rate relations given in Eqn. 6 and appears in the source term vector, H , in Eqn. 1.

$$\begin{aligned} \dot{m}^- &= \frac{C_{dest} \tilde{\rho}_v \alpha_l \text{MIN}[0, p - p_v]}{\frac{1}{2} \rho_\infty U_\infty^2 t_\infty} \\ \dot{m}^+ &= \frac{C_{prod} \tilde{\rho}_v (\alpha_l + \sum_{k=2}^K \alpha_k)^2 \alpha_v}{t_\infty} \end{aligned} \quad (6)$$

In the liquid-vapor mass-transfer model, destruction of liquid is related to the difference of the local pressure, p , and vapor saturation pressure, p_v , and the production of liquid is related to the presumption that condensation is restricted to a heuristic interfacial area (Kunz 2000). For results presented here, thermal effects are not considered, vapor pressure is directly related to cavitation number.

3 RESULTS

Computational results have been obtained for two different open propellers and one ducted pumpjet. The first open propeller has been computationally driven deep into cavitation thrust breakdown. The performance and cavity shape for this condition are compared to experiments. The second open propeller has been run in both steady and unsteady operating conditions. The steady condition is meant to represent operation with a uniform inflow. The unsteady condition is intended to capture operation in a nonuniform wake generated inflow. A third computational investigation is presented for a ducted pump jet. The pump jet is modeled from on-design to the cavitation-driven thrust breakdown condition.

3.1 P4381 (5-BLADED OPEN PROPELLER) STEADY MODELING

A no-skew unducted propeller, designated P4381, was tested by Boswell (1971) as part of a larger effort to parameterize ahead powering, blade-rate, fluctuating loads, cavitation inception, cavitation thrust breakdown, structural integrity, and backing performance with consideration of the effect of blade skew. The cavitation thrust breakdown performance of the propeller was determined in a water tunnel. Measurements were taken at specific advance ratios while incrementally dropping the tunnel operating pressure. This process reduced the test cavitation index in a prescribed fashion. Thus, sufficient data were obtained to complete a map of thrust and torque over a range of advance ratios and cavitation indices.

The computational modeling of cavitation breakdown of P4381 has been undertaken and presented previously (Lindau 2005). Those modeling results were successful in reproducing the measured thrust and torque over a wide range of cavitation indices and advance ratios. However, those efforts did fall short in capturing the correct vaporous cavity shape (as delineated in the CFD solution by an isosurface of constant volume fraction). In that work it was suggested that although thrust and torque were captured quite well, a lack of grid resolution off the blade surface was inhibiting the proper capture of the cavity shape. Due to the great deal of twist typically found in open propeller blades, the production of high quality structured grids can be taxing. This challenge may be somewhat mitigated with the use of overset grids. Therefore, in the present work, the particular case of cavity shape resolution for the P4381 at the advance ratio of 0.7 and cavitation index of 3.5 was undertaken with overset grids. Note that a computational grid study has been previously reported by Lindau (2005). Results at the

advance ratio of 0.7 based on an overset computational mesh are presented in Fig. 1. Here the thrust, Fig. 1(a), and torque, Fig. 1(b), coefficients are plotted against cavitation index. The values up to the point of breakdown agree quite well. The cavitation index corresponding to the onset of breakdown also appears to have been captured nicely. However, the in-breakdown thrust and torque are too low by approximately 20%. The overset computational grid is illustrated on the shaft and blade surface in Fig. 1(c). In this figure, the propeller would rotate in the counterclockwise direction. In Fig. 1(d) the propeller surface, colored by pressure, and cavity shape are shown at the cavitation index of 3.5 and advance ratio of 0.7.

3.2 E779A (4-BLADED OPEN PROPELLER) STEADY AND UNSTEADY MODELING

Steady and unsteady results were obtained for the *Wageningen type*, four bladed propeller, INSEAN E779A (Pereira, et al. 2004). Steady, periodic, cavitating, and single-phase computations are presented in uniform inlet conditions. For the case of a nonuniform inflow, unsteady results are also presented. The E779A is a four-bladed open propeller, which has some slight blade sweep. In the experimental set-up, it is driven by a shaft upstream at constant angular speed. The Reynolds number, based on chord length, was modeled at roughly 2.8 million.

Thrust and torque at a number of single phase conditions and at several different in-cavitation advance ratios have been documented by Pereira et al. (2004). The single-phase and in-cavitation modeled and experimentally obtained thrust and torques are presented in Figure 2. The numerically computed thrust and torque are given for single phase flow at the design advance ratio, $J=0.88$, and for both single-phase and cavitating flow at the highly loaded, $J=0.71$, condition. However, more explanation of the presented computed results is needed. Computational results are given at the exact advance ratios as well as at *corrected* advance ratios. During the modeling effort, in comparison to experiments, it was found that computed single-phase thrust and torques were consistently high. It was subsequently found that by reducing the model rotational speed by 3% from the prescribed value for a given advance ratio, the experimental results were more nearly matched. This was true at a range of advance ratios and suggests that there were improperly modeled elements such as tunnel boundary conditions. Such elements may have resulted in the computed loading to be higher than in the experiments. It should be noted that the actual water tunnel had a rectangular cross section. However, to yield a steady-state solution, it was modeled as circular.

Thus at the *corrected* conditions (running the modeled propeller at 97% of the nominal rotational speed for each advance ratio) the single phase thrust and torque agree quite nicely with experiments. Also in Figure 2, the cavitating flow thrust and torque are presented for a

highly loaded advance ratio ($J=0.71$). In this case the cavitation number, $\sigma_n = (p_\infty - p_v) / (\frac{1}{2} \rho n^2 D^2)$, was 1.76.

In Figure 3, a photograph from the experiments and an illustrated CFD result at the cavitating conditions of $J=0.71$, and $\sigma_n=1.76$ are presented. The modeled cavity is delineated by an isosurface at $\alpha_v=0.9$. Agreement between experiment and computation in cavity shape is evident. Also evident is cavitation in the trailing tip vortex, illustrated by stream traces initiated from the modeled cavity isosurface. Note that the stream traces are colored by vapor volume fraction and scaled from $\alpha_v=0.1$ to 0. It should be considered that the CFD result is presented at the *corrected* $J=0.71$ condition, but the photograph is at the true condition, rotating at approximately 3% greater speed.

In Figure 4, a summary of unsteady results obtained when modeling the E779A in a nonuniform flow field are presented. In Fig. 4(a), the overset computational grid on the solid surfaces is illustrated. The grid is nearly identical to the one used for the steady flow test case. However no periodicity was assumed and the full annulus was modeled. The modeled inflow velocity is shown in Fig. 4(b). The inflow conditions were specified and meant to model an as yet unpublished experiment. The computational results are presented at one advance ratio, $J=0.9$, and three conditions corresponding to one single-phase and two cavitating cases. Currently, only the reported mean operating conditions for the experiments are available for comparison. Those expected mean thrust and torque values are indicated with red dashed lines in Fig. 4(c). The mean values are also expected to be unaffected by the small amount of cavitation present in the modeled cases. The unsteady traces in Fig. 4(c) indicate the thrust and torque histories at the three conditions. In Figure 5, selected snapshots from cavitating modeled conditions are shown. Here the solid surfaces are colored by pressure and the cavity is delineated by a gray isosurface of vapor volume fraction equal to 0.5. Recall that the wake feature affects the flow around top dead center of the rotation (0°). Therefore, each blade becomes highly loaded as it passes through 0° and the loading returns to the more nominal condition outside of that region.

3.3 JHU/NSWC WATERJET PUMP

An axial flow waterjet pump has been designed, fabricated, and tested by researchers from Johns Hopkins University and the Naval Surface Warfare Center (Wu et al. 2008). To allow complete optical access to the blade row passages, the test pump was fabricated out of transparent acrylic and run with a working fluid matching the index of refraction of the acrylic. The single phase and cavitating flow through this pump has been computationally modeled. Results are presented here for a single rotor blade passage. For all conditions presented here, the stator row is modeled with body forces and blockage terms. These source terms were obtained iteratively and should be appropriate for single phase

operation at the determined advance ratio ($J=0.492$). In addition, the inflow to the rotor was assumed to have a slug profile. The outflow pressure profile was maintained at a radial distribution, again, based on the single phase computations. Thus, an improved level of fidelity with experiments should be achievable by:

- 1) Adjusting the stator body forces to match conditions at each different cavitation number.
- 2) Obtaining the inflow velocity profile either from experiments or more extensive modeling of the pump loop.
- 3) Adjusting the outflow pressure profile to match conditions at each different cavitation number.

Adjusting the inflow profile should improve not only the cavitating flow computations but also the single-phase flow analysis. However, it should be noted that based on the plotted single-phase performance map of Wu et al. (2008) the water jet total head rise at $J=0.492$ was 4.1m. The computationally determined total head rise using the tools and computational grid described here is 3.97m, a difference of approximately 1%.

A single advance ratio is modeled at multiple cavitation numbers. This represents thrust breakdown as it might be achieved in a water tunnel test facility. There it is typical for a pump to be run at a constant flow rate and rotational speed (i.e. advance ratio) while the absolute tunnel pressure is reduced. The modeled thrust breakdown performance is shown in Figure 6. Here the thrust, $C_T=T/(\rho U^2 \pi D^2)$, and torque, $C_Q=Q/(\rho U^2 \pi D^3)$, coefficients are plotted. Note that computed thrust and torque are measured on the rotating surfaces only. Note also that for the modeled internal flow path the cavitation number is based on a reference pressure at the exit of the domain. It is clear from the figure that at cavitation numbers greater than 3.4, almost no effect of modeled cavitation is seen on performance. However, as cavitation number (i.e. tunnel pressure) is reduced below 3.4, the thrust and torque are both effected. Thrust drops off steadily as cavitation number is reduced. Although torque drops as well, there is a non monotonic trend in the computed torque as cavitation number is decreased from 3.4 to 2.4. The causes of this seeming anomaly may be evident in the cavity shape, consequent effective blade camber, and flow in the tip gap region.

Illustrated results from selected modeled waterjet flow conditions are shown in Figure 7. Here the rotor and hub surfaces are colored by pressure, the cavity is illustrated by an isosurface at a constant volume fraction of 0.5, and the shroud is illustrated by a translucent grey surface. Note that due to the reference pressure being held constant at the outflow, the effect of cavitation (the effect of reducing $p_{exit}-p_v$) on thrust is evident through the colored pressure levels at the inflow region (on the drive shaft and suction side of the rotor blades). It is also evident that the small amount of tip gap cavitation present in the $\sigma=3.37$ case causes little alteration of flow in the blade passage. However, the massive amount of

cavitation on the suction side in the $\sigma=2.27$ case clearly has a large effect on the rotor blade passage flow, and subsequent loss in flow turning.

4 CONCLUSIONS

A formulation and computational method suitable to modeling turbulent single phase and cavitating flows through marine propulsors has been presented. Results demonstrating the fidelity of the model for single-phase and cavitating flows through an open propeller and a waterjet pump have also been included. Unsteady, open propeller performance appears to match the mean values of experimental data. The presented results serve to demonstrate the capabilities of the method to accurately capture cavity shape and performance of marine propulsors under the influence of large-scale cavitation.

ACKNOWLEDGMENTS

This work was, in part, supported by the Office of Naval Research Grant # N00014-06-1-0643 with Dr. Ki-Han Kim as program officer.

REFERENCES

- Abdol-Hamid, K.S. Lakshmanan, B. Carlson, J.R. (1995) Application of Navier-Stokes Code PAB3D with k-e Turbulence Model to Attached and Separated Flows, NASA Technical Paper 3480, NASA Langley Research Center, Hampton, Virginia.
- Boswell, R.J. (1971) "Design, Cavitation Performance and Open-Water Performance of a Series of Research Skewed Propellers," Naval Ship Research and Development Center, Washington, DC, Report 3339.
- Chorin, A.J. (1967) A numerical method for solving incompressible viscous flow problems, *J. Comput. Phys.* **2**, 12.
- Kinzel, M.P. Lindau, J.W. Kunz, R.F., and L.J. Peltier (2007) "Detached Eddy Simulations for Cavitating Flows," AIAA-2007-4098, 18th Computational Fluid Dynamics Conference, Miami, FL, June 25-28.
- Kunz, R.F., Boger, D.A., Stinebring, D.R., Chyczewski, T.S., Lindau, J.W., Gibeling, H.J., Venkateswaran, S., and T.R. Govindan (2000), "A Preconditioned Navier-Stokes Method for Two-Phase Flows with Application to Cavitation Prediction," *Computers and Fluids*, **29**, pp. 849-875.
- Lindau, J.W. Boger, D.A. Medvitz, R.B. and R.F. Kunz (2005), "Propeller Cavitation Breakdown Analysis," *Journal of Fluids Engineering*, Transactions of ASME, **127**, pp. 995-1002.
- Lindau, J.W., Venkateswaran, S., Kunz, R.F. and C.L. Merkle (2001) "Development of a Fully-Compressible Multiphase Reynolds-Averaged Navier-Stokes Model," AIAA 2001-2648, 15th AIAA Computational Fluid Dynamics Conference, Anaheim, California.
- Noack, R.W. (2005(1)) "SUGGAR: A General Capability for Moving Body Overset Grid Assembly," AIAA-2005-5117, 17th AIAA Computational Fluid Dynamics Conference, Toronto, Ontario.
- Noack, R.W. (2005(2)) "DiRTlib: A Library to Add an Overset Capability to Your Flow Solver," AIAA Paper 2005-5116, 17th AIAA Computational Fluid Dynamics Conference, Toronto, Canada.
- Pereira, F. Salvatore, F. and F.D. Felice (2004) "Measurement and Modeling of Propeller Cavitation in Uniform Inflow," *Journal of Fluids Engineering*, Transactions of ASME, **126**, pp. 671-679, July 2004.
- Strelets, M. (2001) "Detached eddy simulation of massively separated flows," AIAA 2001-0879, 39th Aerospace Sciences Meeting and Exhibit, Reno, Nevada, January, 2001.
- Venkateswaran, S. Lindau, J.W. Kunz, R.F. and C. L. Merkle (2002) "Computation of Multiphase Mixture Flows with Compressibility Effects," *Journal of Computational Physics*, **180**, pp. 54-77.
- Venkateswaran, S. and C. L. Merkle, (1999) "Analysis of Preconditioning Methods for the Euler and Navier-Stokes Equations," VKI Lecture Series 1999-03, Von Karman Institute, Rhode-Saint-Genese, Belgium, March, 1999.
- Wilcox, D.C. (1998) *Turbulence Modeling for CFD*, DCW Industries, La Canada, California.
- Wu, H. Soranna, F. Michael, T. Katz, J. and S. Jessup, (2008) "Cavitation in the Tip Region of the Rotor Blades Within a Waterjet Pump," Proceedings of FEDSM2008, ASME Fluids Engineering Conference, August 10-14, 2008, Jacksonville, Florida, USA

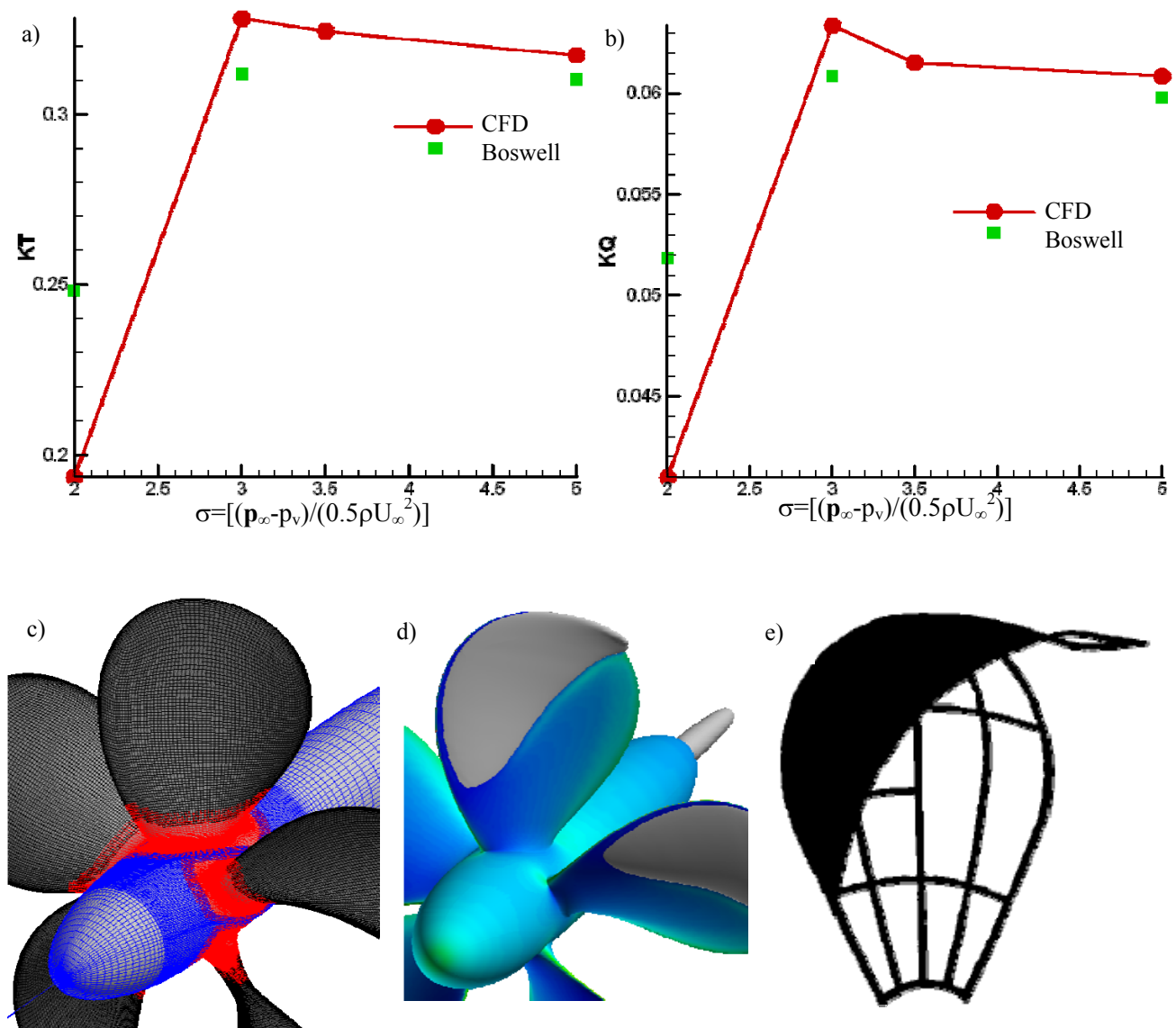


Figure 1: Computations and measurements at the highly loaded ($J=0.7$) condition for the P4381 (Boswell 1971).
 a) Computed (UNCLE-M) and measured (Boswell 1971) thrust coefficient ($K_T=T/(\rho N^2 D^4)$) versus cavitation index.
 b) Computed (UNCLE-M) and measured (Boswell 1971) torque coefficient ($K_Q=Q/(\rho N^2 D^5)$) versus cavitation index.
 c) Computational overset grid illustrated on solid surfaces (replicated about axis for clarity).
 d) Surface colored by pressure and cavity indicated by gray isosurface of vapor volume fraction ($\alpha=0.5$) at cavitation index, $\sigma=3.5$ (replicated about axis for clarity)
 e) Sketch of cavity at this condition ($J=0.7$, $\sigma=3.5$) from Boswell (1971).

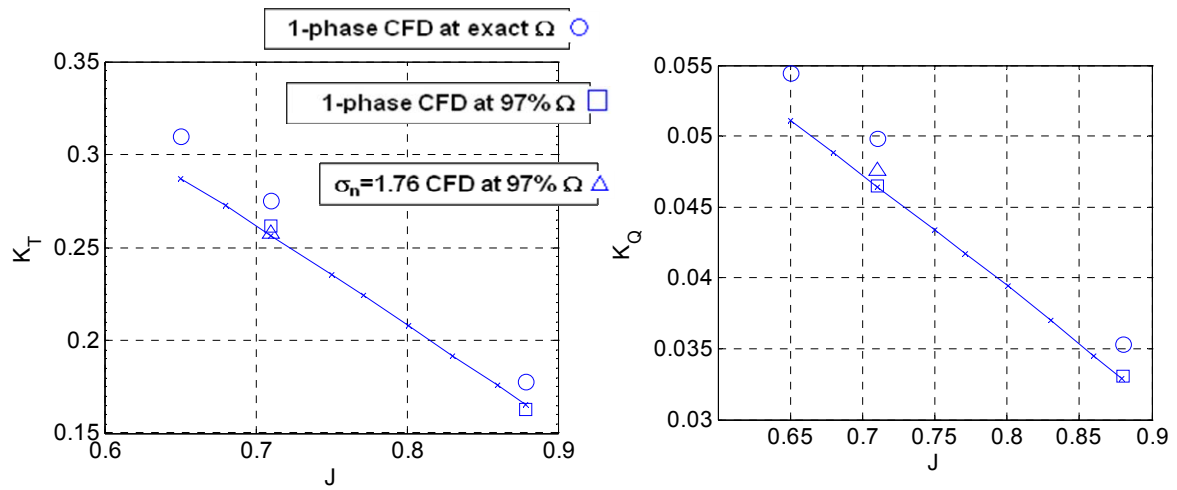


Figure 2: Thrust ($K_T=T/(\rho N^2 D^4)$) and torque ($K_Q=Q/(\rho N^2 D^5)$) at a range of advance ratios for the E779A propeller. Experiments are solid line. Symbols are CFD.

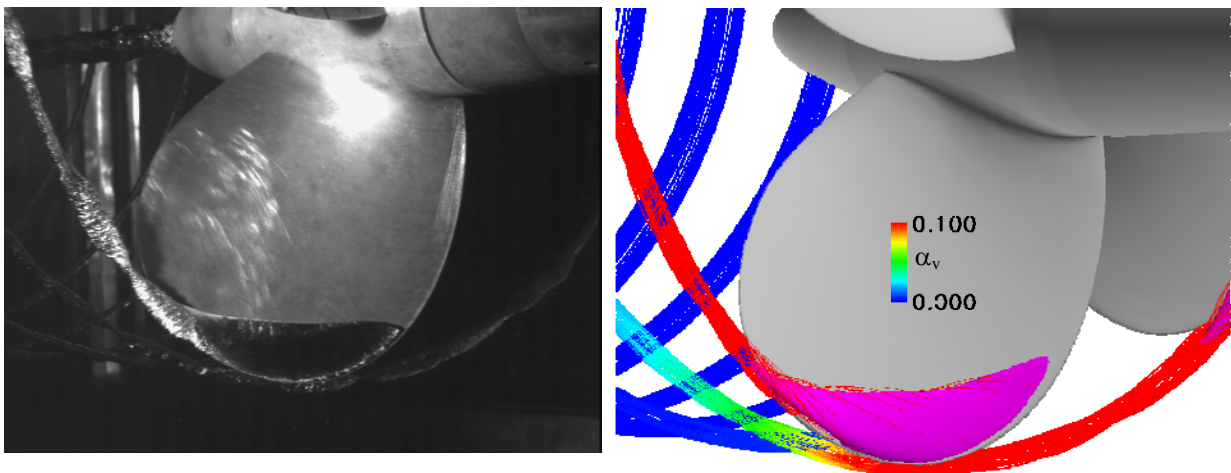


Figure 3: Photograph from experiments (Pereira et al. 2004) and illustrated CFD solution. Flow over the E779A propeller. Solution is illustrated by pink isosurface of vapor volume fraction, $\alpha_v=0.9$. Streamlines emanating from the vapor fraction isosurface are colored by vapor volume fraction.

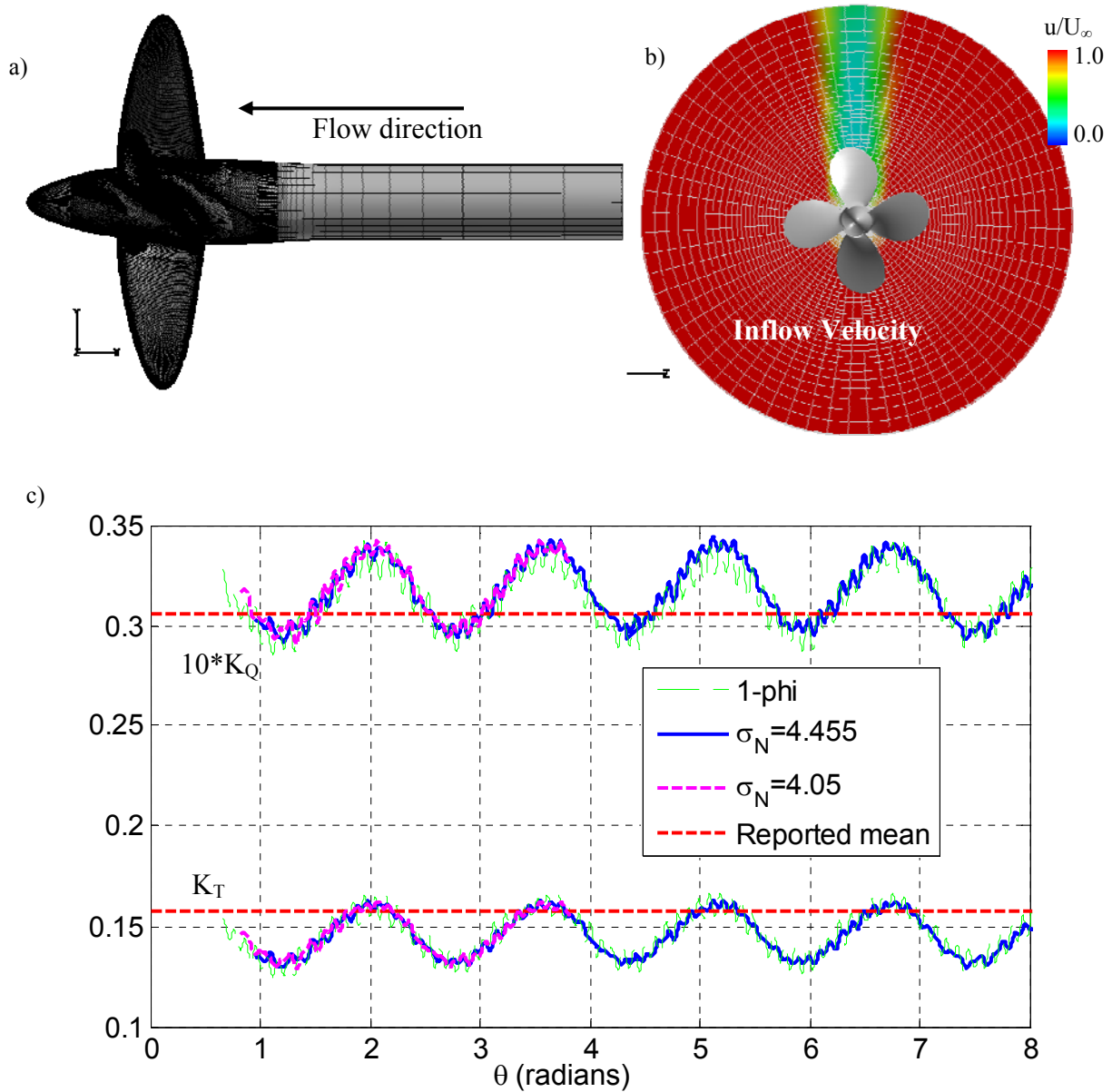


Figure 4: Computational grid, boundary conditions, and integrated quantities from computed unsteady flow over the E779A propeller.

a) Portion of overset computational grid on solid surfaces.

b) Grid at inflow plane illustrating wake. Inflow colored by velocity magnitude relative to the mean free stream value. Propeller surface indicated as in top dead center position.

c) Integrated thrust ($K_T=T/(\rho N^2 D^4)$) and torque ($K_Q=Q/(\rho N^2 D^5)$) at advance ratio, $J=0.9$. Single phase and cavitating conditions. Red dashed lines indicate the expected mean thrust and torques based on experiments.

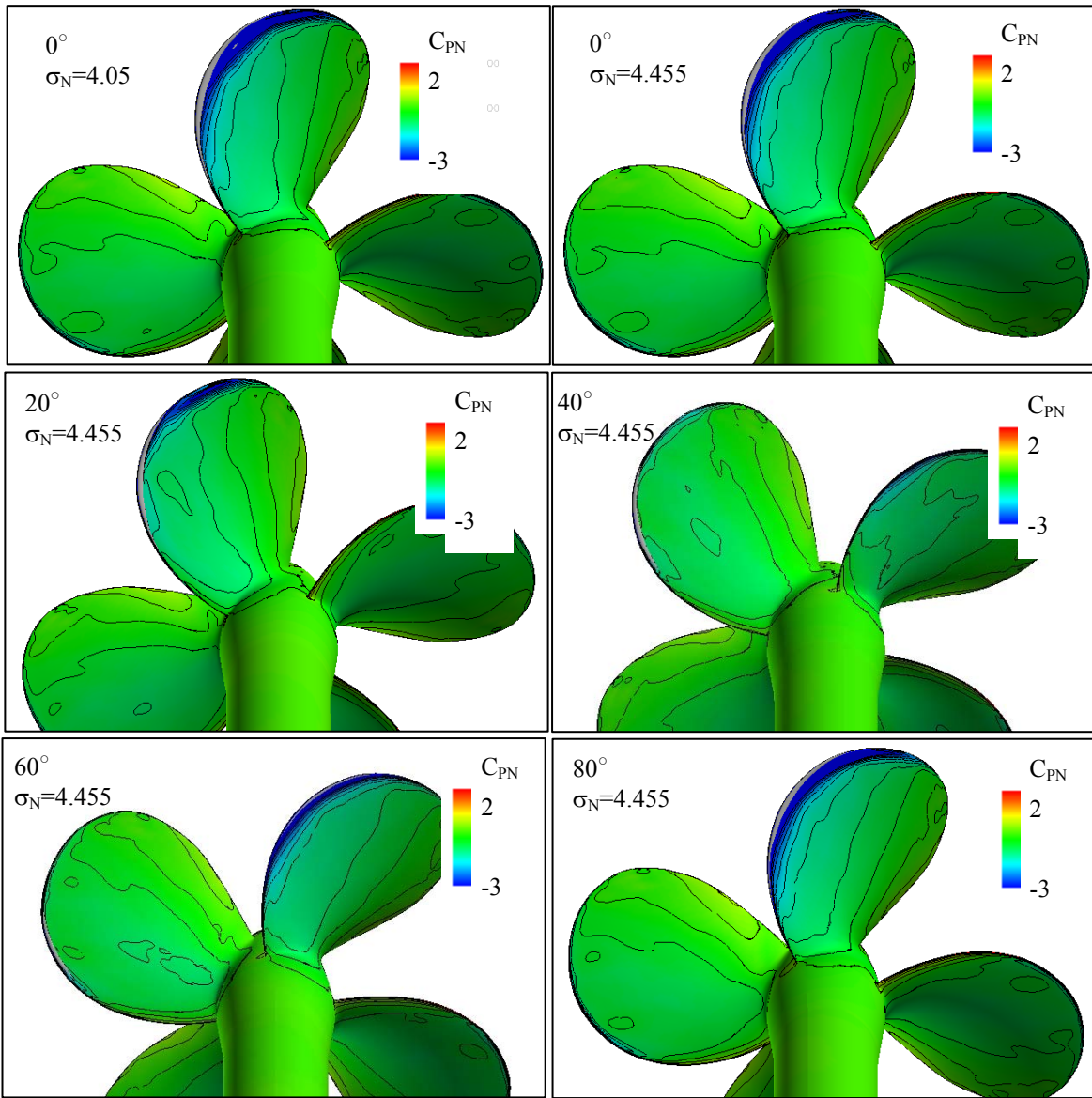


Figure 5: Snapshots from CFD solutions: INSEAN E779A Propeller operating in generated wake. Two cavitation numbers at the top-dead-center position. Followed by a time sequence, the solution at $\sigma_N=4.455$ for angular positions from 20° - 80° after top dead center. $J=0.90$, $sN=4.455$

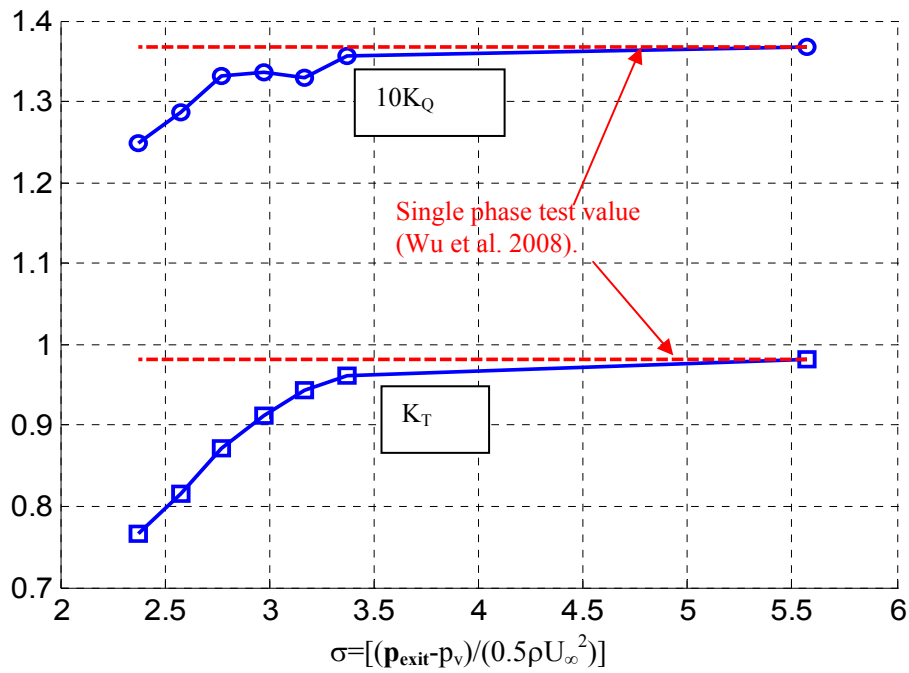


Figure 6: Computed cavitation performance of waterjet pump at running with flow rate of $0.160\text{m}^3/\text{s}$ at a single advance ratio, $J=0.492$. Plotted thrust, $K_T=T/(\rho N^2 D^4)$ and torque $K_Q=Q/(\rho N^2 D^5)$. Based on reported performance (Wu et al. 2008), computed single-phase thrust is within 1% of measurements. Exit pressure is averaged over outflow boundary for each solution.

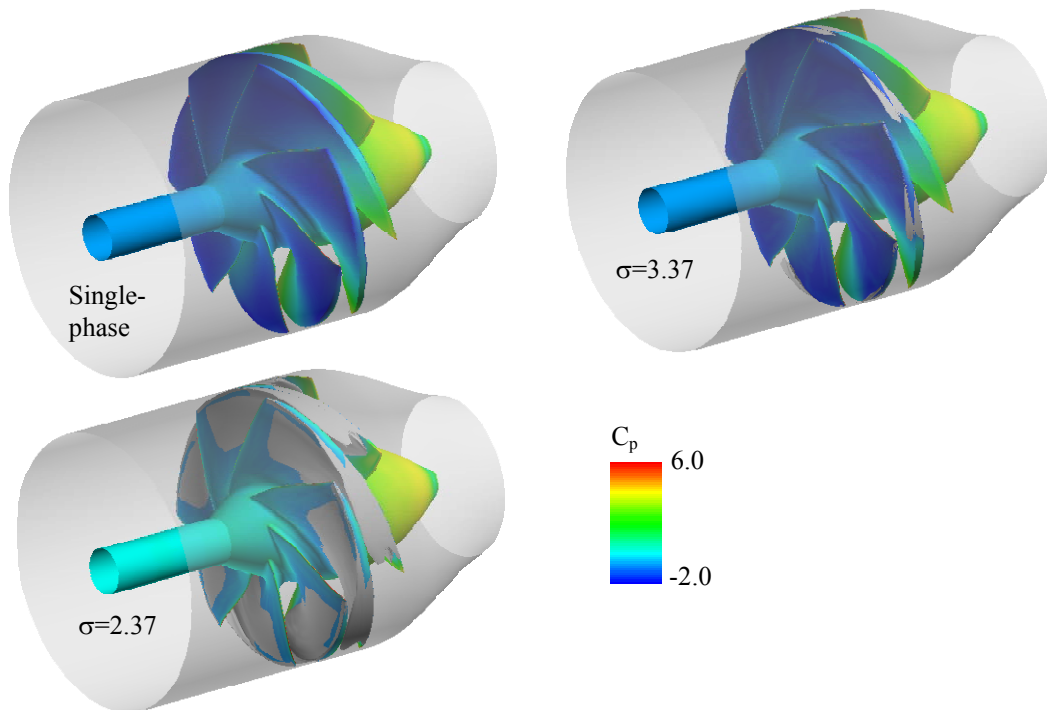


Figure 7: Illustrated results from computed cavitating flow through waterjet rotor at advance ratio, $J=0.492$. Downstream stator forces and blockage effects are modeled. Full rotor and stationary hub are colored by pressure. Shroud is illustrated by translucent grey surface. Cavity is illustrated by a grey isosurface at a vapor volume of 0.5. Nominal free stream velocity is 3.658m/s . Cavitation number and pressure coefficient are referenced to mean rotor exit boundary pressure $[\sigma=(p_{\text{exit}}-p_v)/(0.5\rho U_\infty^2)]$.